Mode hybridization in DNA-inspired helical metamaterials with variable centro-asymmetry

Gunho Kim[1], Kaila M. Y. Coimbra[1], and Chiara Daraio[1,*]

[1,*]Division of Engineering and Applied Science, California Institute of Technology, Pasadena, CA 91125, USA

1 Ladder-like analytical model

1.1 Effective stiffness and mass

The effective stiffness and mass of both the longitudinal mode and the torsional mode of the helical metamaterials (HMMs) are derived from the long-wave properties of the representative volume element (RVE). The slope of the longitudinal branch and the torsional branch at the origin of the dispersion curves (Fig. 2(d)) corresponds to the wave speed of each mode under long-wave approximation. The mass, M, and the moment of inertia with respect to the central axis, J, of a single horizontal beam are acquired by integrating the density (with or without a vector from the center axis) over volume. The effective longitudinal stiffness, K, and the torsional stiffness, herein denoted as C, of the unit cell is derived from the relation $c_l = a_{RVE}\sqrt{\frac{K}{M}}$ or $c_t = a_{RVE}\sqrt{\frac{C}{J}}$, where $a_{RVE} = 1$ cm. All the derived properties and corresponding wave speeds for the longitudinal mode and the torsional mode are tabulated in Table S1.

Table S1: Wave speeds from the dispersion curves are calculated under long wavelength assumption. Corresponding effective stiffness and mass of the RVE of the HMMs for longitudinal modes and torsional modes are listed below.

Effective parameters	Longitudinal mode	Torsional mode
Wave speed, c [m/s], via long-wave approximation	422.18	65.77
Mass, M [kg]	1.65×10^{-3}	-
Moment of inertia, J [kg·m^2]	-	1.30×10^{-7}
Stiffness, K [N/m]	2.93×10^{6}	-
Torsional stiffness, C [N·m/rad]	-	5.61

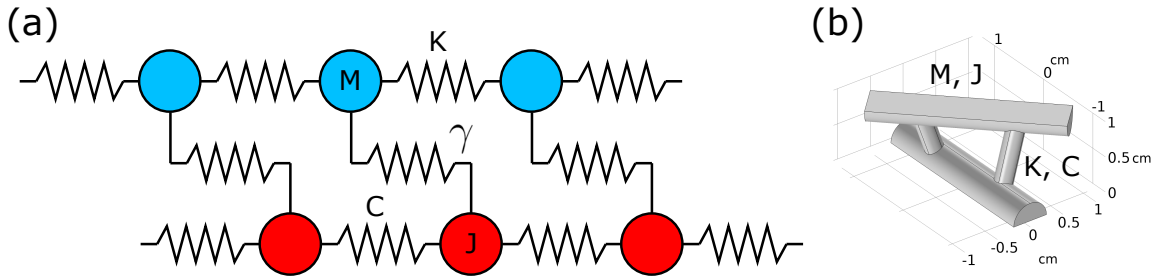

Figure S1: (Color Online) (a) A ladder-like meta chain model with a mass M, stiffness K, moment of inertia J, torsional rigidity C, and coupling stiffness γ. (b) A representative volume element of the HMMs used for the analytical model.

1.2 Derivation of the analytical model

We analyze a parallel mass-spring model [1] (Fig. S1(a)) using the effective parameters of the RVE derived in the previous section. For direct comparison, we divide the torsional stiffness C and the moment of inertia J by a correction factor, $\frac{1}{2}r^2$, to match their units to N/m and kg, respectively. The radius of the vertical pillars, r, is used for the correction factor, based on the relation between the moment of inertia of the vertical cylinder with its mass, $\frac{J}{m} = \frac{1}{2}r^2$. The equations of motion of a parallel mass-spring model are:

$$\begin{aligned} Mu_j + K(2u_j - u_{j-1} - u_{j+1}) + \gamma(u_j - v_j) = 0, \\ Jv_j + C(2v_j - v_{j-1} - v_{j+1}) + \gamma(v_j - u_j) = 0. \end{aligned} \tag{S1}$$

Here, u_j and v_j represent the displacements of the j-th M and J, and are assumed to be in harmonic forms:

$$\begin{aligned} u_j(t) = \tilde{u}(k(\omega))e^{i(kjd-\omega t)}, \\ v_j(t) = \tilde{v}(k(\omega))e^{i(kjd-\omega t)}. \end{aligned} \tag{S2}$$

We then insert the values of the effective parameters to the equations of motion, to derive the dispersion curves for the parallel mass-spring model. The coupling coefficient γ is obtained so that the y-intercept of the upper branch of the analytical dispersion curves fits the edge of the longitudinal branch (at $k = 0$) in the FE analysis. The dispersion curves of the parallel mass-spring model with varying coupling stiffness γ are plotted together with the numerical dispersion curves, in Fig. 2(d-f). When $\gamma = 0$, the longitudinal mode and the torsional mode of the analytical model have no interaction, acting as two independent branches. However, as γ increases in value, we observe an avoided crossing from the two branches, which suggests increased coupling [2].

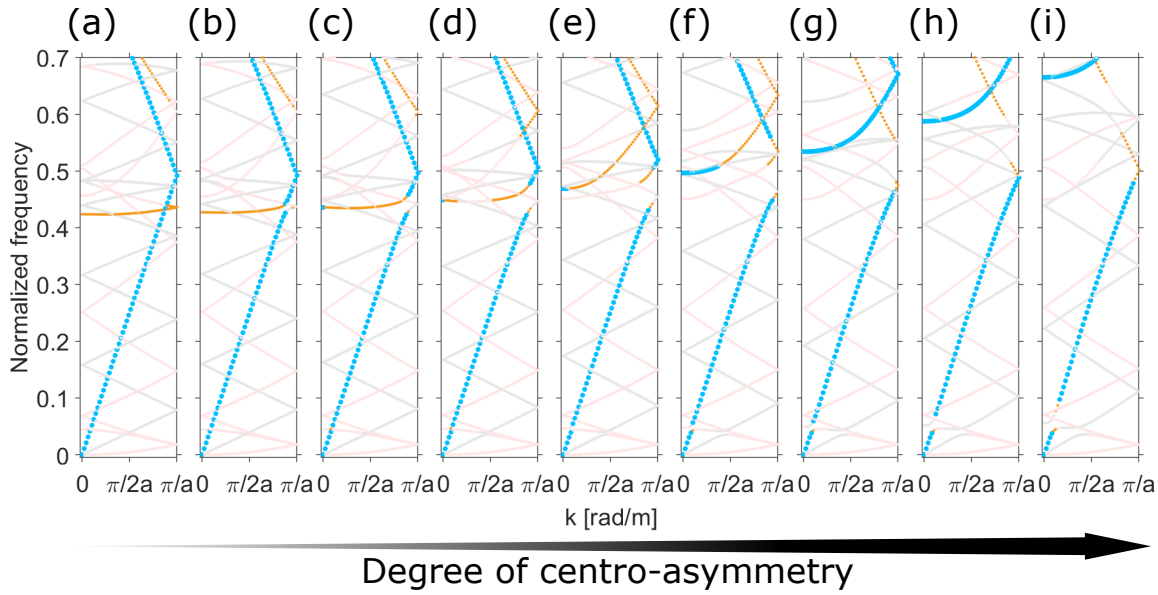

Figure S2: (Color Online) Dispersion curves of the HMMs with increasing degree of centro-asymmetry: (a) 50-50 (centrosymmetric), (b) 43.25-56.25, (c) 37.5-62.5, (d) 31.25-68.75, (e) 25-75, (f) 18.75-81.25, (g) 12.5-87.5, (h) 6.25-93.75, and (i) 0-100 (fully centro-asymmetric) material distribution. The longitudinal modes (blue) and the transitional modes (orange) are highlighted to show the evolution of longitudinal band gaps.

2 Development of the longitudinal band gap

2.1 Dispersion curves with increasing degree of centro-asymmetry

To study the evolution of the longitudinal band gap with an increasing level of centro-asymmetry, we create finite element models with varying center of mass. The material distribution of stainless steel inserts change from 50-50 distribution (centrosymmetric) to 0-100 distribution (full centro-asymmetric) with intermediate steps. As the center of mass of the horizontal mass beams moves further away from the central axis of the HMMs, the longitudinal band gap shifts upward and widens as shown in Fig. S2. This is due to the stronger coupling between the longitudinal mode and the rest of the modes with increased degree of centro-asymmetry. When the HMMs are centro-symmetric (Fig. S2(a)), the longitudinal branch remains linear even though the transitional branch horizontally crosses the longitudinal branch at the frequency around 0.45. As the centro-asymmetry of the HMMs intensifies, the coupling between the transitional mode and the longitudinal mode gets stronger, creating the longitudinal band gap which widens as well (Fig. S2(b-d)). This trend becomes more complicated as the longitudinal mode couples with multiple transitional branches (Fig. S2(e,f)). With even higher degree of centro-asymmetry, an avoided crossing between two separate longitudinal branches forms the larger longitudinal band gap (Fig. S2(g-i)).

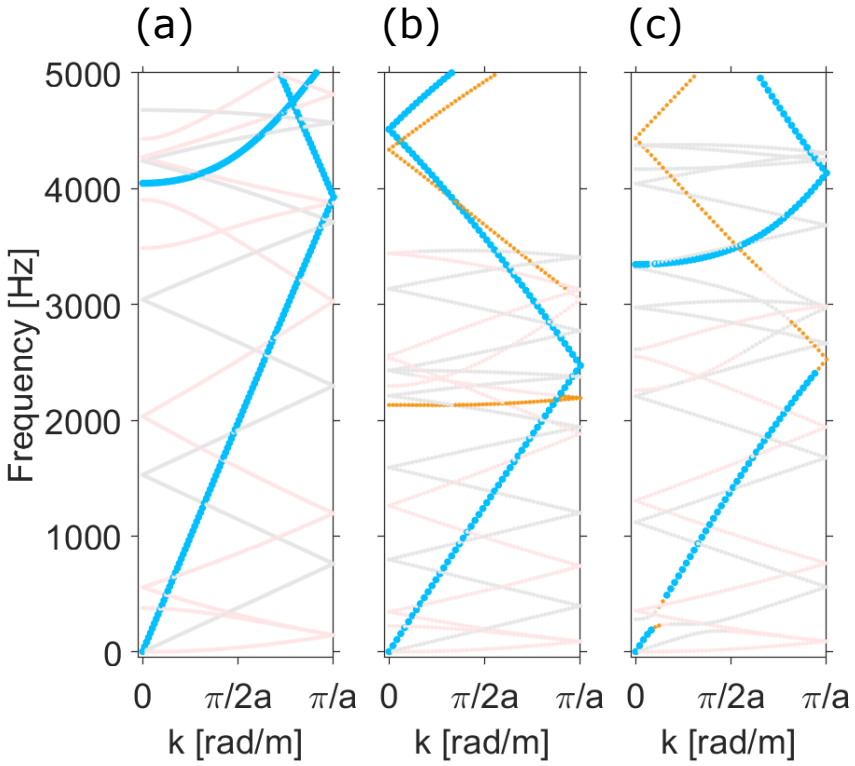

Figure S3: (Color Online) Dispersion curves of the (a) centrosymmetric HMMs with same material inserts as the base material, (b) centrosymmetric HMMs with heavier stainless steel inserts, and (c) fully centro-asymmetric HMMs with heavier stainless steel inserts. The longitudinal modes (blue) and the transitional modes (orange) are highlighted to show the evolution of longitudinal band gaps. The color of the torsional mode (black) and the rotaional modes (red) are suppressed in the background.

2.2 Dispersion curves with increasing density of the inserts

We study the dispersion curves of HMMs with inserts, varying their density and distribution, to characterize the hybridization mechanism (Fig. S3). Three different types of HMMs are investigated: (i) centrosymmetric HMMs with same material inserts as the base material, (ii) centrosymmetric HMMs with heavier stainless steel inserts, and (iii) fully centro-asymmetric HMMs with heavier stainless steel inserts. Both centrosymmetric cases show that the longitudinal mode is not hybridized with other modes in the low frequency regime, regardless of the inserts' density (Fig. S3(a,b)). A subwavelength bandgap forms only when centro-asymmetry is introduced, at the point where the longitudinal branch first crosses the rotational branch. Such results imply that hybridization is induced by the asymmetric distribution of mass, and not by the increased mass of the inclusions. This mode hybridization leads to the longitudinal subwavelength band gap, which occurs due to the local resonance of the unit cell [3].

References

[1] Setare Hajarolasvadi and Ahmed E. Elbanna. Dispersion properties and dynamics of ladder-like meta-chains. *Extreme Mechanics Letters*, 43:101133, 2021.

[2] Brian R. Mace and Elisabetta Manconi. Wave motion and dispersion phenomena: Veering, locking and strong coupling effects. *The Journal of the Acoustical Society of America*, 131(2):1015–1028, 2012.

[3] Zhengyou Liu, Xixiang Zhang, Yiwei Mao, Y Y Zhu, Zhiyu Yang, C. T. Chan, and Ping Sheng. Locally Resonant Sonic Materials. *Science*, 289(September):1734–1736, 2000.